Journal of Materials Chemistry B

ROYAL SOCIETY OF CHEMISTRY

PAPER

View Article Online
View Journal | View Issue

Cite this: J. Mater. Chem. B, 2020, 8, 3655

Stretchable gold fiber-based wearable electrochemical sensor toward pH monitoring†

Ren Wang,[ab] Qingfeng Zhai,[ab] Yunmeng Zhao,[ab] Tiance An,[ab] Shu Gong,[ab] Zhirui Guo,[ab] QianQian Shi,[ab] Zijun Yong[ab] and Wenlong Cheng *[ab]

Received 4th November 2019,
Accepted 7th January 2020

DOI: 10.1039/c9tb02477h

rsc.li/materials-b

Sweat pH is a key health indicator related to metabolism and homeostasis level through hydrogen ion concentration in biological bio-fluid. Therefore, increasing research efforts have been directed to develop wearable pH sensors towards continuous non-invasive monitoring of sweat pH values in the out-of-hospital environments. Herein, we report a stretchable gold fiber-based electrochemical pH sensor based on our recently developed elastomer-bonded gold nanowire coating technology. The densely packed gold film offers superior strain-insensitive conductivity, high stretchability and large electrochemical active surface area (EASA). By electrodepositing polyamine (PANI) and Ag/AgCl onto the gold fibers, we could selectively detect the pH based on open circuit potentials in an ion-selective electrode design. The obtained fiber-based pH sensors feature a great sensitivity (60.6 mV per pH), high selectivity against cationic interference and high stretchability (up to 100% strain). One of the attributes for the fiber-based sensors is that they can be weaved into textiles, holding great potential for integration into everyday clothing for "unfeelable" personal health monitoring.

Introduction

Wearable chemical sensors have attracted tremendous attention in the past several years due to their promising applications in the continuous monitoring of sweat non-invasively.[1–4] Sweat is secreted by the sweat gland beneath our skin, which contains a wealth of biometric information to reflect the deep health status of the body at the molecular level. Among various indicators, pH reflects the metabolism and homeostasis level through the hydrogen ion concentration in bio-fluids that sustain life. Abnormal pH levels in bio-fluids may indicate dysfunctions or diseases such as diabetes, kidney stone or cystic fibrosis.[5,6] In addition, the pH value is slightly acidic at normal skin condition, whereas it is slightly alkaline at the wound area due to the numerous enzymes and bacteria. The different stages of the wound healing process can be described by specific and dynamic pH variation as well.[7,8] Therefore, continuous and *in situ* pH monitoring from sweat can offer great benefits in the treatment of the aforementioned diseases. In comparison to other analytical tools, electrochemistry is advantageous because of facile miniaturized design and integration with state-of-the-art mobile technology. Among the various analytical methods, electrochemical potentiometric measurement is a preferred choice for pH monitoring due to its reliability and wide sensing range.[9]

Recently, impressive achievements have been made in the wearable electrochemical pH sensors.[10–15] For instance, an electrochemical patch-based pH sensor array was fabricated on a PET substrate, showing high sensitivity to pH change by conformal contact with the skin.[16] A wearable fabric device has been developed by weaving different functionalized CNT fibers into a smart textile for real-time monitoring of pH, ions and glucose.[17] It has to be noted that most of the reported pH sensors show limited intrinsic stretchability because of the use of a relatively rigid substrate and/or rigid electrode materials. Our skins undergo routine stretching in normal life (for example, 30% stretching for arm area and 80% stretching for elbow area), therefore, it is beneficial to develop highly stretchable pH sensors to maintain the sensing performance under severe mechanical deformation.[18] In this context, besides soft sensors on other flexible substrates,[19,20] fiber-based electrochemical sensors are advantageous as they can be woven into textiles and everyday clothing for continuous and *in situ* pH monitoring from human sweat without interfering with daily activities.[21,22]

Our group has recently developed a powerful yet general elastomer-coating strategy that can be used to grow vertical gold nanowire films on a wide range of polymeric substrates including PET, Ecoflex, PDMS, latex, nitrile glove, and styrene-ethylene/butylene-styrene (SEBS).[23,24] The coating is conformal

[a] Department of Chemical Engineering, Faculty of Engineering, Monash University, Clayton 3800, Victoria, Australia. E-mail: wenlong.cheng@monash.edu
[b] The Melbourne Centre for Nanofabrication, 151 Wellington Road, Clayton 3168, Victoria, Australia

† Electronic supplementary information (ESI) available. See DOI: 10.1039/c9tb02477h

to planar sheets or fibers.[25] In comparison to other active materials, gold is regarded as an ideal wearable electrode material interfacing with body fluids due to its high electrical conductivity, superior mechanical compliance, ease of modification, high chemical resistance, wide electrochemical window and excellent biocompatibility required for on-skin and in-body applications.[26,27] In our initial studies, we have successfully demonstrated wearable glucose sensors based on gold nanowire patches[28] and fibers[29] as well as integrated multisensor arrays.[30] All those reported electrochemical biosensing systems are based on the standard three-electrode design, in which redox enzymes are used to achieve specific detection.

Herein, we further extend our stretchable gold fiber-based electrochemical biosensors to the two-electrode system towards pH detection, in which the working electrode is made from dry-spun elastic gold fibers coated with PANI and the reference electrode is the Ag/AgCl-coated gold fiber. Unlike the three-electrode system, the counter electrode is not required in the two-electrode potentiometric system that measures open-circuit potentials, particularly suitable for sensitive and selective ion detections. With this ion-selective electrode (ISE) design, our fiber-based pH sensor exhibited a typical sensitivity of 60.6 mV per pH and 100% stretchability with negligible influence on the sensitivity. Furthermore, the fiber-based sensors were woven into a wearable textile matrix for detecting pH in artificial sweat, which showed only 2.6% variation in sensitivity upon a strain of up to 30%. These encouraging results indicate the potential of our gold fibers as smart wearable textiles to be used in the next-generation soft wearable sensors for pH monitoring anytime, anywhere.

Result and discussion

Fabrication and characterization of the elastomer gold fiber

Fig. 1a illustrates the fabrication process of our elastomeric gold fibers, with regards to both the pH-sensing working electrode and the reference electrode preparation steps. The elastomeric gold fibers were fabricated by a dry spinning process based on our previous study.[25,29] We firstly synthesized oleylamine (OA) capped ultrathin AuNWs with a diameter of ~2 nm and an aspect ratio of more than 10 000, which was proved by TEM characterization (Fig. S1, ESI†). Then, the AuNWs were mixed with SEBS in tetrahydrofuran (THF), followed by a dry spinning process under ambient conditions. The AuNWs/SEBS fiber underwent a pre-strain, and then was immersed into Au electroless growth solution, followed by sodium borohydride ($NaBH_4$) treatment. This process led to highly conductive, strain-insensitive gold fibers.[25] X-ray powder diffraction (XRD) was carried out before and after the Au film growth, with the corresponding XRD patterns shown in Fig. S2 (ESI†). Both patterns can be identified to typical face-centered cubic lattice structures, demonstrating that the surface-coated gold films had similar crystalline structures to that of the embedded gold nanowires.

We measured the EASA by performing cyclic voltammetry (CV) at a scan rate of 0.1 V s^{-1} in 1 M H_2SO_4 solution. As shown

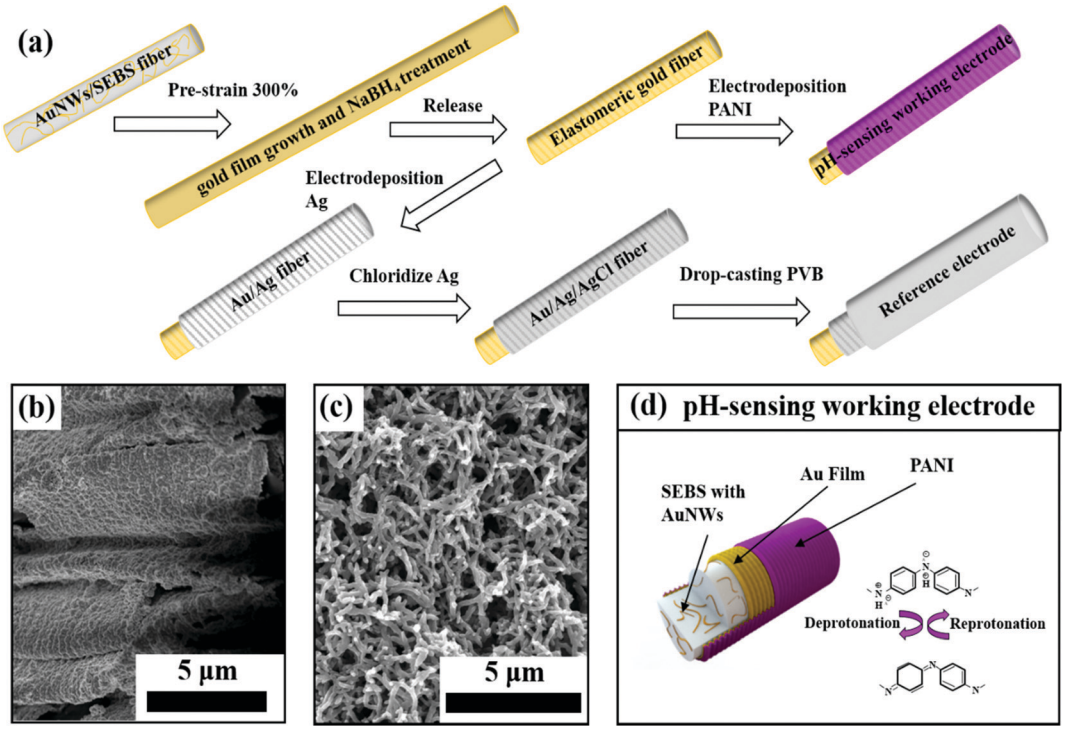

Fig. 1 (a) Scheme of the fabrication process of fiber-based pH-sensing working electrode and reference electrode. (b) and (c) are SEM images of the elastomeric Au fiber surface before and after PANI electrodeposition, respectively. (d) The structure and mechanism of the obtained pH working electrode.

in Fig. S3 (ESI†), the typical oxidation and reduction peaks of gold (1.3 V and 0.9 V) can be clearly identified. The EASA was calculated according to eqn (1) and (2):

$$\text{EASA} = Q/C \quad (1)$$

$$Q = A/v \quad (2)$$

where Q is the charge required for the reduction of the Au oxide formed in the positive scan, C is the required charge for the reduction of a monolayer of Au oxide (386 μC cm^{-2}), A is the reduction current peak area and v is the scan rate.[31,32] With this approach, the estimated EASA is 0.51 cm^2 compared with the gold fiber geometric area (GA) of the fiber surface (0.0377 cm^2), which was enhanced by 13.53 times. These properties are advantageous for electrochemical applications.

Fabrication of fiber-based working and reference electrodes

After elastomeric gold fiber fabrication, a layer of PANI was electrodeposited onto the gold fiber surface by electrochemical polymerization (Fig. S4, ESI†). This process led to conformal PANI coating with percolating nanofiber morphologies. It is known that pre-strained gold fibers have wrinkled microstructure (Fig. 1b). It appears that the microgroves have been filled with PANI, clearly seen from the SEM characterization as shown in Fig. 1c. Raman spectra were further used for characterizing the elastomeric gold fiber (Fig. S5, ESI†). Before PANI electrodeposition, the two prominent peaks at 1078 cm^{-1} and 1589 cm^{-1} were attributed to the ν(C–C) breathing modes of benzene ring, proving the presence of residual 4-mercaptobenzoic acid (MBA) on the gold film surface. After PANI deposition, these two characteristic peaks disappeared. Instead, a set of Raman peaks characteristic of PANI was observed. This indicates fully conformal coverage of PANI on the elastomeric gold fiber, in agreement with the SEM images. With PANI deposition, the gold fiber changed color from light golden to dark blue with a slight increase in the fiber diameter (Fig. S6, ESI†).

The PANI modified gold fiber can serve as an ISE for pH detection (Fig. 1d). The hydrogen ion can be detected *via* deprotonation and reprotonation process of PANI, leading to the changes in open circuit potential (OCP) *versus* a reference electrode. According to the Nernst equation, pH is defined as negative logarithm base 10 of hydrogen ion activity[33] and the theoretical pH sensitivity limit is 59.1 mV per pH at room temperature calculated by Nernst equation.[34]

To detect pH reliably, it is important to design a reference electrode with a constant potential, which can be obtained through the electrochemical deposition of Ag onto the gold fiber surface using CV followed by chlorination into AgCl (Fig. S7a and b, ESI†). Afterwards, a layer of polyvinyl butyral (PVB) is further drop-casted on the surface of the reference electrode to minimize the potential drift and isolate undesirable ion adsorption to the electrode surface. As seen in Fig. S7c (ESI†), the OCP of Au/Ag/AgCl fiber *versus* commercial Ag/AgCl reference electrode was very stable after PVB coating while the electrode without PVB coating exhibited an obvious potential drift under the same condition. This is because the PVB membrane can exchange specific electrolytes while separating other ions in solution to provide a stable OCP value.[35]

Performance evaluation of the fiber-based pH sensor

The aforementioned PANI decorated gold fiber and the Ag/AgCl@gold fibers could be assembled to serve as a stretchable pH sensor. The pH-sensing performances were investigated by immersing these two electrodes into McIlvaine's buffer (about 5 mm depth) in the pH range from 4 to 8, which is the typical pH range of human sweat. As shown in Fig. 2a, the potential was quantitatively decreasing with the increase in pH at room temperature. Further numerical fitting (Fig. 2b) yielded a good linear relationship between the potential and pH in the sensing range from 4 to 8 with the sensitivity of 60.6 mV per pH (R^2 = 0.997), which is very close to the theoretically predicted pH sensitivity using Nernst equation. Moreover, the gold fiber-based pH sensor also exhibited excellent selectivity. As shown in Fig. 2c, the pH sensor showed good response to hydrogen ion, while no potential changes were observed after adding the interfering ions including NH_4^+, Ca^{2+}, Mg^{2+} and Na^+. In addition, the pH sensor also exhibited excellent repeatability with a relative standard deviation (RSD) of ~3% in one complete cycle from pH 4 to 8 (Fig. 2d). Long-term operational stability was also investigated by keeping the obtained fiber-based pH sensor in McIlvaine's buffer (pH = 6) for 8000 seconds at room temperature. The results show negligible variation in potential with a value of less than 5 mV (Fig. S8, ESI†).

We further evaluated the pH-sensing performance of the gold fiber-based pH sensor under stretching conditions. As shown in Fig. 3a, the fiber-based sensor can be stretched up to 100% directly and back to the initial length without any observable structural changes. Fig. 3b illustrates the OCP potential values of the pH sensor under the applied strains

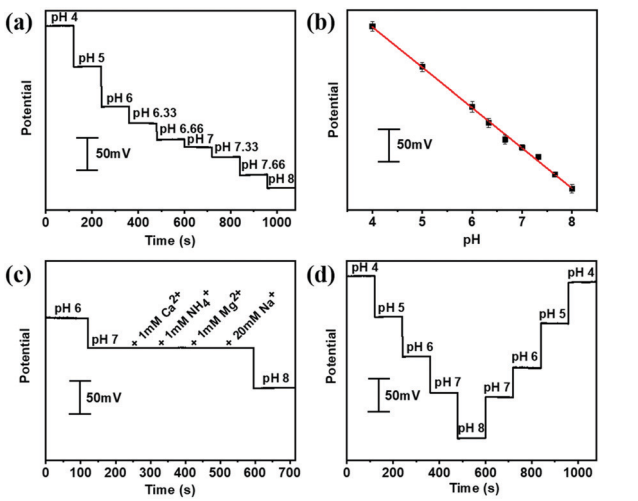

Fig. 2 The electrochemical performance of Au/PANI fiber-based pH sensor in standard McIlvaynes buffers *versus* Au/Ag/AgCl reference electrode. (a) The open circuit potential performance of fiber-based pH sensor to different pH ranging from 4 to 8. (b) Calibration curves for pH sensor. (c) The selectivity of fiber-based pH sensor. (d) The repeated performance of fiber-based pH sensor in one complete cycle from pH 4 to 8.

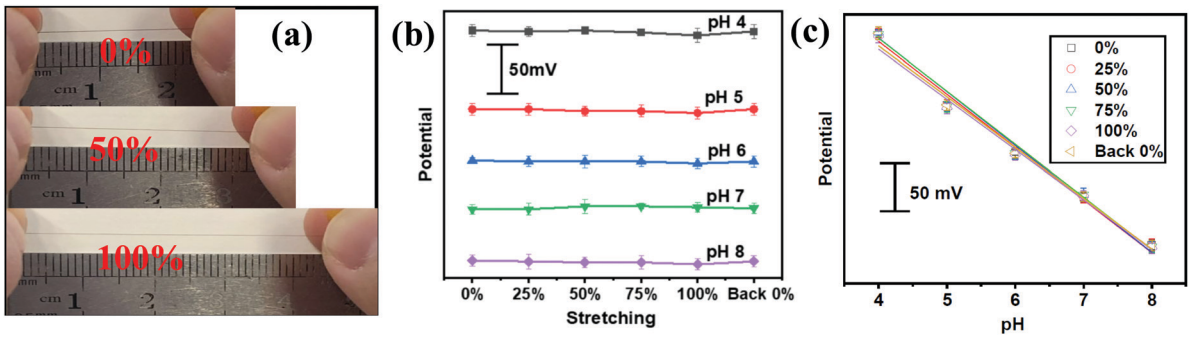

Fig. 3 The stretchable performance of Au/PANI fiber-based pH sensor in standard McIlvaynes buffers. (a) Digital images of elastomer Au fiber under 0%, 50% and 100% stretching state. (b) The OCP performance of the stretchable fiber-based pH sensor response to different stretching states from 0% to 100% and back to 0% in pH ranging from 4 to 8. (c) The linear relationship of stretchable fiber-based pH sensor at different stretching states.

from 0% to 100% and back to 0% in different solutions with pH ranging from 4 to 8. It can be seen that the OCP potential only shows minimal deviation (<3%) at 100% strain.

The high performance may originate from the fiber-like PANI film, which can maintain good conductivity pathways under stretched states. To prove this hypothesis, we directly stretched fiber-based pH working electrodes to 100% strain. At this stretching state, only small cracks on the fiber surface was observed but the PANI film maintained the overall structural integrity without delamination of the Au film (Fig. S9a and b, ESI†). The minimal structural changes in PANI structures could be recovered upon strain release (Fig. S9c, ESI†). This explains the small variation (~6.5%) in the sensitivity between stretched and initial states (Fig. 3c).

In addition, we compared the performance of our gold fiber-based pH sensor with previously reported flexible wearable pH sensors, as shown in the Table S1 (ESI†). Although our sensor isn't the most sensitive, it represents the most stretchable pH sensor. The simultaneously achieved high sensitivity and high stretchability indicate the great potential of our gold fiber-based pH sensor in next generation soft wearable electronics.

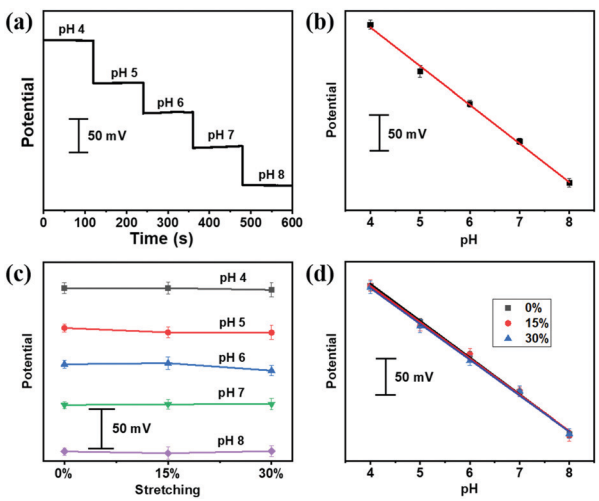

Fig. 4 The electrochemical and stretchable performance of pH smart textile in artificial sweat pH range from 4–8. (a) The OCP performance of the fiber-based pH sensor. (b) Linear calibration plot of the pH sensor. (c) The OCP performance of the stretchable smart pH textile response to different stretching states from 0% to 30%. (d) The linear relationship of stretchable smart pH textile at 0% to 30% stretching states.

Integration of the fiber-based sensor into textile and detection of pH of artificial sweat

Our stretchable fiber-based pH sensor could be easily weaved into a textile matrix (Fig. S10, ESI†), which could serve as wearable sensors for the pH detection of artificial sweat, containing NH_4Cl, urea, $CaCl_2$, $MgCl_2$, KCl, NaCl, uric acid, glucose and lactate with varying pH. As shown in Fig. 4a, the OCP potential responds reliably to different pH from pH 4 to 8 of the artificial sweat, following a linear relationship fitting (Fig. 4b). A linear regression gave rise to a sensitivity of 53.4 mV per pH (R^2 = 0.997). After applying different strains, the OCP potential was measured under different pH values from 4 to 8, as shown in Fig. 4c. Encouragingly, the pH sensitivity of the textile sensor did not deteriorate under deformed states (Fig. 4d), indicating the potential application for on-body personal pH monitoring.

Conclusions

In summary, we have successfully fabricated a stretchable ISE pH sensor based on elastomeric gold fiber. The as-fabricated fiber-based ISE sensors have shown excellent detection performances towards pH with sensitivity (60.6 mV per pH), selectivity, linear pH range of 4 to 8, and high intrinsic stretchability (up to 100%). The fiber-based pH sensors could be weaved into textiles, showing comparable sensing performances in artificial sweat. In comparison to other active materials for pH detection, our gold fibers achieved the highest intrinsic stretchability. This attribute, in conjunction with other features of gold materials such as high biocompatibility, chemical inertness under body fluidic conditions, facile surface modification by Au-thiol chemistry, and wide electrochemical sensing windows, indicate the great potential of our gold fibers as next-generation smart textile for non-invasive, continuous monitoring of biological health markers.

Experimental section

Chemicals and materials

Gold chloride trihydrate ($HAuCl_4 \cdot 3H_2O$), $NaBH_4$, OA, triisopropylsilane (TIPS), silicon oil, L-ascorbic acid (L-AA), MBA, NaCl, KCl, $CaCl_2$, $MgCl_2$, NH_4Cl, KNO_3, $AgNO_3$, Na_2HPO_4, urea, uric acid, glucose, lactate, citric acid, PVB, aniline were purchased from Sigma-Aldrich. SEBS (G1651H) was purchased from Kraton. *n*-Hexane and methanol were purchased from Merck. THF and ethanol were purchased from Thermo Fisher Scientific. H_2SO_4 and HCl were purchased from JT Baker. Standard McIlvaynes buffer solutions were prepared by mixing various amounts of 0.2 M Na_2HPO_4 with citric acid to obtain desired pH (from 4 to 8). Artificial sweat containing 3 mM NH_4Cl, 22 mM urea, 0.4 mM $CaCl_2$, 50 μM $MgCl_2$, 10 mM KCl, 137 mM NaCl, 25 μM uric acid, 100 μM glucose and 5 mM lactate with varying pH was used. All the chemicals were at least analytical grade without conducting any purification process and the Milli-Q water (resistivity more than 18 MΩ cm^{-1}) was used in all the experiments.

Preparation of elastomer gold fibers

The elastomer gold fiber was fabricated according to our previous study with a little modification.[25] Briefly, $HAuCl_4 \cdot 3H_2O$ (29.3 mg), OA (1 mL) and TIPS (1.4 mL) were added to *n*-hexane (30 mL) successively and mixed; the colour of the solution changed to clear red orange. After keeping at room temperature for more than 12 hours without light, the colour turned to dark red, indicating that the ultrathin AuNWs were successfully synthesized. Then, the above OA capped AuNWs were mixed with ethanol and centrifuged for removing the OA ligand. The final AuNWs (15 mg) were re-dispersed in THF (2 mL) and mixed with SEBS (200 mg) and silicon oil (20 mg) and homo-dispersed. The mixed solution was transferred into a syringe and extruded into air, leaving Au/SEBS elastomer fibers (non-conducting), due to the rapid drying of THF at room temperature. Finally, the Au/SEBS elastomer fiber with 300% pre-strain was immersed into Au electroless growth solution (12 mM $HAuCl_4 \cdot 3H_2O$, 1.1 mM MBA ethanol solution, 29.1 mM L-AA water solution) for 10 min followed by immersing into 25 mM $NaBH_4$ aqueous solution for 15 min to remove the MBA ligand, which lead the AuNPs to fuse into Au films and greatly enhance the conductivity.[23] After releasing the pre-strained fiber to initial length, the elastomeric gold fiber was successfully fabricated. As the AuNWs embedded into the fiber acted as seed for Au film growth, the wrinkled structure of Au film is strongly bonded to the elastomeric fiber surface. The resistance of gold elastomer fiber is 25–50 Ω cm^{-1}. Then, the electrochemical performance of the fiber was tested using CV at 0.1 V s^{-1} until stable by immerging it into 1 M H_2SO_4.

Preparation of the pH-sensing working electrode

PANI was deposited onto the surface of gold fibers through an electrochemical method and served as the pH-sensing working electrode. CV was carried out in 0.1 M aniline (in 1 M H_2SO_4 solution) electrolyte by scanning from −0.2 to 1 V for 30 cycles at a scan rate of 0.1 V s^{-1}.

Preparation of the Au/Ag/AgCl reference electrode

The Ag/AgCl based gold fiber was used as the reference electrode in pH sensing electrochemical systems. Firstly, a layer of Ag was electrodeposited onto the Au fiber surface by an electrochemical method by scanning from −0.9 to 0.9 V in 5 mM $AgNO_3$/1 M KNO_3 solution for 14 cycles at a scan rate of 0.1 V s^{-1}. Then, the chlorination process was carried out in 10 mM KCl/0.1 M HCl solution using CV by scanning from −0.15 to 1.05 V for 4 cycles at the scan rate of 0.05 V s^{-1}. After drying, a layer of PVB (6 μL) containing NaCl (79.1 mg PVB, 50 mg NaCl that dissolved in 1 mL methanol solution) was drop-casted onto the fiber electrode.

Characterization of sensing fibers

The sensing performances of the fabricated Au fiber based pH sensor at different stretched states (from 0% to 100%) were carried out in standard McIlvaynes buffer solutions and artificial sweat by real-time monitoring the change of OCP for 120 seconds. In addition, the selectivity of the pH sensor was tested in McIlvaynes buffer solutions by successively adding the potential interfering ions with a final concentration of 1 mM $CaCl_2$, 1 mM NH_4Cl, 1 mM $MgCl_2$, and 20 mM NaCl. All the electrochemical testing was performed at an electrochemical workstation (Versa STAT, Princeton Applied Research). The structure of the fiber was characterized by SEM (FEI Helios Nanolab 600 FIB-SEM) and the structure of OA capped AuNWs was characterized by TEM (Philips CM 20). XRD patterns were recorded on a Rigaku Miniflex600 powder diffractometer with Cu Kα radiation (λ = 1.54056 Å) from 20 to 90°. Raman spectra were recorded by a Renishaw RM 2000 Confocal micro Raman system with an excitation laser wavelength of 830 nm, spot size of 1 μm, and laser power of 0.1 mW.

Conflicts of interest

There is no conflict to declare.

Acknowledgements

This research was financially supported under Australian Research Council's. Discovery Projects funding scheme (DP180101715, DP170102208 and LP160100521). This work was performed in part at the Melbourne Centre for Nanofabrication (MCN) in the Victorian Node of the Australian National Fabrication Facility (ANFF).

Notes and references

1 J. Kim, A. S. Campbell, B. E. de Avila and J. Wang, *Nat. Biotechnol.*, 2019, **37**, 389–406.
2 M. Bariya, H. Y. Y. Nyein and A. Javey, *Nat. Electron.*, 2018, **1**, 160–171.
3 Y. Yang and W. Gao, *Chem. Soc. Rev.*, 2019, **48**, 1465–1491.
4 W. Gao, S. Emaminejad, H. Y. Y. Nyein, S. Challa, K. Chen, A. Peck, H. M. Fahad, H. Ota, H. Shiraki, D. Kiriya,

D. H. Lien, G. A. Brooks, R. W. Davis and A. Javey, *Nature*, 2016, **529**, 509–514.
5 N. M. Maalouf, M. A. Cameron, O. W. Moe and K. Sakhaee, *Clin. J. Am. Soc. Nephrol.*, 2010, **5**, 1277–1281.
6 W. Dang, L. Manjakkal, W. T. Navaraj, L. Lorenzelli, V. Vinciguerra and R. Dahiya, *Biosens. Bioelectron.*, 2018, **107**, 192–202.
7 T. Guinovart, G. Valdés-Ramírez, J. R. Windmiller, F. J. Andrade and J. Wang, *Electroanalysis*, 2014, **26**, 1345–1353.
8 R. Rahimi, M. Ochoa, T. Parupudi, X. Zhao, I. K. Yazdi, M. R. Dokmeci, A. Tamayol, A. Khademhosseini and B. Ziaie, *Sens. Actuators, B*, 2016, **229**, 609–617.
9 E. Bakker, P. Bühlmann and E. Pretsch, *Chem. Rev.*, 1997, **97**, 3083–3132.
10 A. J. Bandodkar, V. W. Hung, W. Jia, G. Valdes-Ramirez, J. R. Windmiller, A. G. Martinez, J. Ramirez, G. Chan, K. Kerman and J. Wang, *Analyst*, 2013, **138**, 123–128.
11 S. Nakata, M. Shiomi, Y. Fujita, T. Arie, S. Akita and K. Takei, *Nat. Electron.*, 2018, **1**, 596–603.
12 M. Bariya, Z. Shahpar, H. Park, J. Sun, Y. Jung, W. Gao, H. Y. Y. Nyein, T. S. Liaw, L. C. Tai, Q. P. Ngo, M. Chao, Y. Zhao, M. Hettick, G. Cho and A. Javey, *ACS Nano*, 2018, **12**, 6978–6987.
13 R. Rahimi, M. Ochoa, A. Tamayol, S. Khalili, A. Khademhosseini and B. Ziaie, *ACS Appl. Mater. Interfaces*, 2017, **9**, 9015–9023.
14 S. Nakata, T. Arie, S. Akita and K. Takei, *ACS Sens.*, 2017, **2**, 443–448.
15 L. Manjakkal, W. Dang, N. Yogeswaran and R. Dahiya, *Biosensors*, 2019, **9**, 14.
16 H. Y. Nyein, W. Gao, Z. Shahpar, S. Emaminejad, S. Challa, K. Chen, H. M. Fahad, L. C. Tai, H. Ota, R. W. Davis and A. Javey, *ACS Nano*, 2016, **10**, 7216–7224.
17 L. Wang, L. Wang, Y. Zhang, J. Pan, S. Li, X. Sun, B. Zhang and H. Peng, *Adv. Funct. Mater.*, 2018, 28.
18 J. Lee, B. Llerena Zambrano, J. Woo, K. Yoon and T. Lee, *Adv. Mater.*, 2019, 1902532.
19 S. Gong, D. T. Lai, Y. Wang, L. W. Yap, K. J. Si, Q. Shi, N. N. Jason, T. Sridhar, H. Uddin and W. Cheng, *ACS Appl. Mater. Interfaces*, 2015, **7**, 19700–19708.
20 Y. Zhang, L. Zhang, K. Cui, S. Ge, X. Cheng, M. Yan, J. Yu and H. Liu, *Adv. Mater.*, 2018, **30**, e1801588.
21 W. Zeng, L. Shu, Q. Li, S. Chen, F. Wang and X. M. Tao, *Adv. Mater.*, 2014, **26**, 5310–5336.
22 W. Weng, P. Chen, S. He, X. Sun and H. Peng, *Angew. Chem., Int. Ed.*, 2016, **55**, 6140–6169.
23 Y. Wang, S. Gong, D. Gomez, Y. Ling, L. W. Yap, G. P. Simon and W. Cheng, *ACS Nano*, 2018, **12**, 8717–8722.
24 Y. Wang, S. Gong, S. J. Wang, X. Yang, Y. Ling, L. W. Yap, D. Dong, G. P. Simon and W. Cheng, *ACS Nano*, 2018, **12**, 9742–9749.
25 Y. Zhao, D. Dong, S. Gong, L. Brassart, Y. Wang, T. An and W. Cheng, *Adv. Electron. Mater.*, 2019, **5**, 1800462.
26 Q. Zhai and W. Cheng, *Mater. Today Nano*, 2019, **7**, 100041.
27 B. Zhu, S. Gong and W. Cheng, *Chem. Soc. Rev.*, 2019, **48**, 1668–1711.
28 Q. Zhai, S. Gong, Y. Wang, Q. Lyu, Y. Liu, Y. Ling, J. Wang, G. P. Simon and W. Cheng, *ACS Appl. Mater. Interfaces*, 2019, **11**, 9724–9729.
29 Y. Zhao, Q. Zhai, D. Dong, T. An, S. Gong, Q. Shi and W. Cheng, *Anal. Chem.*, 2019, **91**, 6569–6576.
30 S. Gong, L. W. Yap, B. Zhu, Q. Zhai, Y. Liu, Q. Lyu, K. Wang, M. Yang, Y. Ling, D. T. H. Lai, F. Marzbanrad and W. Cheng, *Adv. Mater.*, 2019, **31**, e1903789.
31 S. Trasatti and O. A. Petrii, *Pure Appl. Chem.*, 1991, **63**, 711–734.
32 F. Jia, C. Yu, Z. Ai and L. Zhang, *Chem. Mater.*, 2007, **19**, 3648–3653.
33 M. I. Khan, K. Mukherjee, R. Shoukat and H. Dong, *Microsyst. Technol.*, 2017, **23**, 4391–4404.
34 A. K. Covington, R. G. Bates and R. A. Durst, *Pure Appl. Chem.*, 1985, **57**, 531–542.
35 T. Guinovart, G. A. Crespo, F. X. Rius and F. J. Andrade, *Anal. Chim. Acta*, 2014, **821**, 72–80.

